

A Practical Approach for Modeling a Bevel Gear

Brendan Bijonowski

The geometry of the bevel gear is quite complicated to describe mathematically, and much of the overall surface topology of the tooth flank is dependent on the machine settings and cutting method employed. AGMA 929-A06—*Calculation of Bevel Gear Top Land and Guidance on Cutter Edge Radius*—lays out a practical approach for predicting the approximate top-land thicknesses at certain points of interest—regardless of the exact machine settings that will generate the tooth form. The points of interest that AGMA 929-A06 address consist of toe, mean, heel, and point of involute lengthwise curvature. The following method expands upon the concepts described in AGMA 929-A06 to allow the user to calculate not only the top-land thickness, but the more general case as well, i.e.—normal tooth thickness anywhere along the face and profile of the bevel gear tooth. This method does not rely on any additional machine settings; only basic geometry of the cutter, blank, and teeth are required to calculate fairly accurate tooth thicknesses. The tooth thicknesses are then transformed into a point cloud describing both the convex and concave flanks in a global, Cartesian coordinate system. These points can be utilized in any modern computer-aided design software package to assist in the generation of a 3D solid model; all pertinent tooth macrogeometry can be closely simulated using this technique. A case study will be presented evaluating the accuracy of the point cloud data compared to a physical part.

Introduction

The first question that comes to mind from any engineer presented by this paper is why would anyone be interested in a close approximation to the tooth flanks of a straight or spiral bevel gear? It is a valid question. A bevel gear designer is typically interested in the minute details of the tooth flank's surface topology to gain the optimized contact conditions under loads that the bevel gears will operate. The method presented in this paper does not address any of these needs.

Purpose

One of the main purposes of this method is to create a working 3D model for visual interrogation of fits and proportions. The bevel designer is typically concerned with the proportions of a myriad of geometric values describing the basic layout of the tooth form. Many of the values like top land balance, slot width tapers, spiral angle adjustments, etc., are hard to visualize for the engineer, and their impact on the tooth form can be drastic.

Thus the gear engineer's toolkit should include a method for generating a 3D model of a bevel gear, as dependency upon CAD for the general engineer is rapidly increasing. Many application engineers are demanded to provide 3D models to their customers. These customers then utilize their CAD system to validate fits and clearances between components in their systems. Gears should not be left out of this analysis. Advancements in 5- and 6-axis machining of gears are rapidly approaching the precision and capability of dedicated gear generating machines; most of these machining centers require a 3D model for programming. If the application engineer provides

a fully developed gear model to the customer, the 5- or 6-axis machining techniques may become very attractive. For this case alone, many gear companies opt out of providing models of their designs.

Background

The method outlined in AGMA 929-A06—*Calculation of Bevel Gear Top Land and Guidance on Cutter Edge Radius*—describes how to calculate the top land thickness for a bevel tooth at specific points of interest; these points of interest are at the toe, mean, heel, and the point-of- involute lengthwise curvature.

Reasons regarding the purpose for these calculation points are beyond the scope of this document. The formulas inside AGMA 929 can be generalized so that a set of equations can be devised to calculate the normal circular tooth thickness anywhere along the profile and length of the tooth.

Why this method is approximate. Given, as stated, that the geometry of a spiral bevel gear is mathematically complicated, the machine settings used to create a spiral bevel gear—whether using face milling or face hobbing—adjust the final flank form of the teeth. A thorough understanding of the machine settings and motions is necessary to achieve an accurate tooth model. AGMA 929-A06 uses the technique of a virtual spur gear to approximate the profile of a bevel tooth in the normal plane, without knowing the motions of the machine generating the final form. In doing so, the tooth thicknesses can be calculated quite simply using traditional methods for spur gears.

The virtual spur gear technique assumes that the tooth form will follow an involute in the profile direction in the normal

plane. This is only a close approximation to the true form of a spiral bevel tooth. Most spiral bevels follow the octoid tooth form, which is similar — but not identical — to the involute tooth form found on most cylindrical gears.

What is missing in AGMA 929-A06 to complete a model. A generalized set of equations can be produced from the content of AGMA 929-A06 to calculate the normal tooth thicknesses of a bevel tooth anywhere in the profile or lengthwise direction. The purpose of this document is to fill in the gaps of AGMA 929-A06 so that a model can be generated. The majority of the content of this document pertains to how the normal tooth thicknesses are oriented in three dimensions and resolves these thicknesses into an array of Cartesian coordinates. (See Figure 1 for a visual depiction of the calculation method described within this document.) Additional information regarding the terminology described within the figure is in the subsequent sections.

This method's shortcomings. Enough has been presented to illuminate the reader as to why this method creates only an approximate method, but there are additional shortcomings worth mentioning. This method does not currently address the root fillet. The coordinates calculated in this method are strictly points following the involute curve that describes the approximate flank form. Coordinates for the root fillet are beyond the scope of this document.

The other major shortcoming is that all subsequent formulas are for spiral bevel gears — without a hypoid offset. Additional provisions would need to be made to generalize the formulas to account for hypoids.

Coordinate System Definition

All bevel gears are designed using a reference right cone called the “pitch cone.” The pitch cone is used as a basis for describing all other geometric entities of the bevel gear. Since describing the motions of the generating process in three dimensions would be hard to visualize or comprehend, the general practice is to un-wrap the surface of the pitch cone into a tangent plane — or “pitch plane.”

The point at the top of the pitch cone is called the “pitch apex.” The pitch apex is significant because the axes of both gear and pinion intersect at this point. Figure 2 displays the pitch cone, the pitch plane unwrapped, and also describes the global Cartesian coordinate system, C_G . Figure 2 also shows the pitch cone sectioned through the YZ plane. This describes the definition of the pitch angle, Γ , and the face width, F — of a part. The global coordinate system follows the right-hand rule and its origin is located at the pitch apex of the member being modeled.

Basic Generation

The majority of all generated spiral bevel gears are manufactured in one of two processes, i.e. — face milling or face hobbing; both manufacturing methods have advantages and disadvantages. For the purposes of this method, a brief understanding of the generating method utilized during these processes is necessary to realize the 3D model.

Face milling. The face milling manufacturing method employs a circular, cup-shaped cutting tool moving in a timed relationship with the workpiece to roll through the gear blank and generate an individual slot. The cutter is then withdrawn,

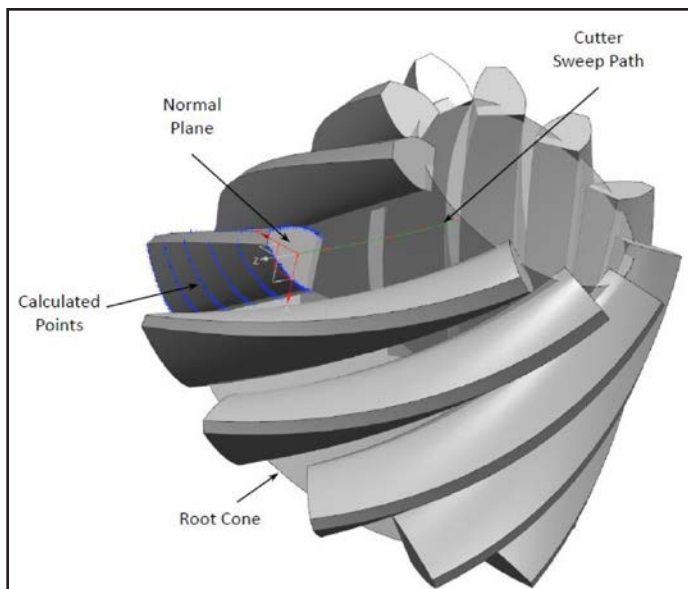


Figure 1 Visual depiction of calculation method.

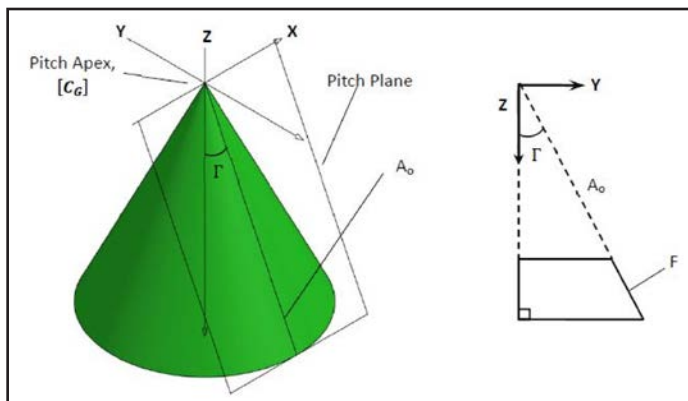


Figure 2 Pitch cone.

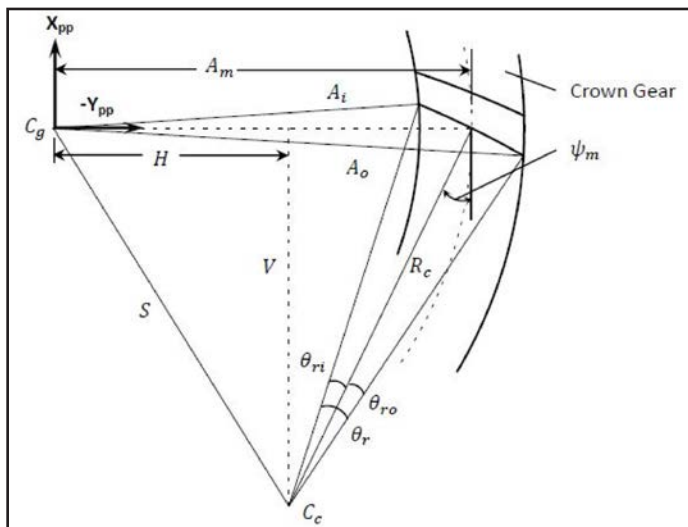


Figure 3 Generating triangle in pitch plane for face milling.

the work is indexed to the location of the next slot, and the process repeated. See Figure 3.

Figure 3 displays three instances of the cutter as it passes through the workpiece; these points are at the toe, mean, and heel of the crown gear. The path of the cutter sweeps a circular arc in the lengthwise direction, with the same radius as the radius of the cutter, R_c . The axis of the crown gear, C_g , is known as the machine center. The local coordinate system for the pitch plane is located at the machine center. X_{pp} correlates to X and Y_{pp} lies along the line describing A_o in Figure 2.

The cutter axis, C_c . This location can be found by:

$$V = R_c \cos \psi_m \quad (1)$$

$$H = A_m - R_c \sin \psi_m \quad (2)$$

$$C_c = (V, H) \quad (3)$$

$$\lambda = \frac{\pi}{2}$$

The sign of the vertical term, V , may either be positive or negative, depending on the hand of spiral to be modeled. Figure 3 shows a right-hand member (use negative value for V when calculating left-hand members). The cutter sweep angle, θ_r , is necessary to determine how much rotation is used during the cutting process. When calculating points to model the gear tooth, these will be the endpoints of the working portion of the cutter path.

$$S = \sqrt{V^2 + H^2} \quad (4)$$

$$\theta_r = \cos^{-1} \left[\frac{S^2 + R_c^2 - A_o^2}{2SR_c} \right] - \cos^{-1} \left[\frac{S^2 + R_c^2 - A_i^2}{2SR_c} \right] \quad (5)$$

$$\theta_{ro} = \cos^{-1} \left[\frac{S^2 + R_c^2 - A_o^2}{2SR_c} \right] - \cos^{-1} \left[\frac{S^2 + R_c^2 - A_m^2}{2SR_c} \right] \quad (6)$$

$$\theta_{ri} = \theta_r - \theta_{ro} \quad (7)$$

Discrete points can be calculated along the cutter sweep on the pitch plane. Using the general parametric formulas for a circle, the solution for a point, p , along the cutter path is:

$$p_x(t) = V + R_c \cos t \quad (8)$$

$$p_y(t) = V + R_c \sin t \quad (9)$$

Where t is a parameter that has the following ranges:

For left-hand members,
$$\pi + \psi_m - \theta_{ri} \leq t \leq \pi + \psi_m - \theta_{ro} \quad (10)$$

For right-hand members,
$$2\pi + \psi_m - \theta_{ri} \leq t \leq 2\pi + \psi_m - \theta_{ro} \quad (11)$$

This cutter path can be broken into as many discrete sections as desired.

Face hobbing. The face hobbing manufacturing method is a continuously indexing process. The cutting tool has groups of staggered blades; the workpiece moves in a timed relationship with the cutter so that a group of blades in the cutter passes through a slot of the workpiece. The face hobbing method generates an extended epicycloidal shape in the lengthwise direction. See Figure 4. for a detailed layout of the face hobbing generating triangle.

Since the lengthwise shape of a face hobbed part creates an extended, epicycloidal shape, a little trigonometry is necessary to calculate the discrete points along the path created by the cutter.

The crown gear tooth count,
$$N_c = \frac{N}{\sin \Gamma} \quad (12)$$

The lead angle of the cutter,
$$v = \sin^{-1} \left[\frac{A_m N_c \cos \psi_m}{R_c N_c} \right] \quad (13)$$

The first auxiliary angle,
$$\lambda = \frac{\pi}{2} \quad (14)$$

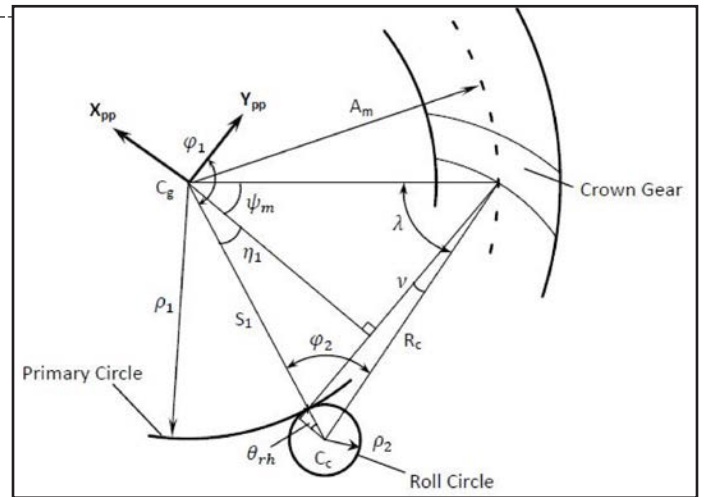


Figure 4 Generating triangle in pitch plane for face hobbing.

The center distance from crown gear center to cutter (Radial),
$$S_1 = \sqrt{A_m^2 + R_c^2 - 2A_m R_c \cos \lambda} \quad (15)$$

The second auxiliary angle,
$$\eta = \cos^{-1} \left[\frac{A_m \cos \psi_m (N_c + N_s)}{S_1 N_c} \right] \quad (16)$$

The second roll angle,
$$\phi_2 = \pi - \eta_1 - \psi_m - \lambda \quad (17)$$

The auxiliary roll angle,
$$\theta_{rh} = \frac{\pi}{2} - v + \phi_2 \quad (18)$$

The radius of the roll circle,
$$\rho_2 = \frac{R_c \cos v}{\cos \theta_{rh}} \quad (19)$$

The radius of the primary circle,
$$\rho_2 = S_1 - \rho_2 \quad (20)$$

The first roll angle (assuming rolling without sliding),
$$\phi_1 = \phi_2 \frac{\rho_2}{\rho_1} \quad (21)$$

Now that the dimensions of the cutting cycle's epicycloid, the cutter path, can be calculated, it would be very difficult to determine the angle of sweep that the cutter makes during the generating process because the cutter axis does not remain stationary during the cutting cycle. The face width of the bevel gear being modeled will be subdivided into discrete portions; the roll angles need to be recalculated for each discrete location individually.

The second roll angle as a function of cone distance, (22)

$$\varphi_{p2}(A_\mu) = \cos^{-1} \left[\frac{S_1^2 + R_c^2 - A_\mu^2}{2S_1R_c} \right]$$

Where,

$$A_i \leq A_\mu \leq A_o \quad (23)$$

The first roll angle as a function of cone distance, (24)

$$\varphi_{p1}(A_\mu) = \varphi_{p2}(A_\mu) \frac{\rho_2}{\rho_1}$$

The local Cartesian coordinates describing a point, p , along the cutter sweep path can be calculated. (25)

$$p_x = -R_c \sin(\varphi_{p1} + \varphi_{p2}) + (\rho_1 + \rho_2) \sin \varphi_{p1} \quad (26)$$

$$p_y = -R_c \cos(\varphi_{p1} + \varphi_{p2}) + (\rho_1 + \rho_2) \cos \varphi_{p1}$$

Wrapping the Pitch Plane

The pitch plane is a tangent plane to the lateral surface of a right cone. This cone, as described earlier, is the "pitch cone." The diagrams take into account the set-up of the machine, the cutter size, and the motion of the cutter. Rotation of the workpiece also needs to be accounted for; this is accomplished by wrapping the pitch plane around the pitch cone. This transforms the local coordinates calculated for the cutter sweep path into global coordinates. These points in the global coordinates will define the center of a tooth slot. The following formulas will transform a point, p , from the local $X_{pp}Y_{pp}$ plane to the global Cartesian coordinate system, C_G .

The first step is to determine the location of the point in the global Z axis direction, (27)

$$z_p = \sqrt{p_x^2 + p_y^2} \cos \Gamma$$

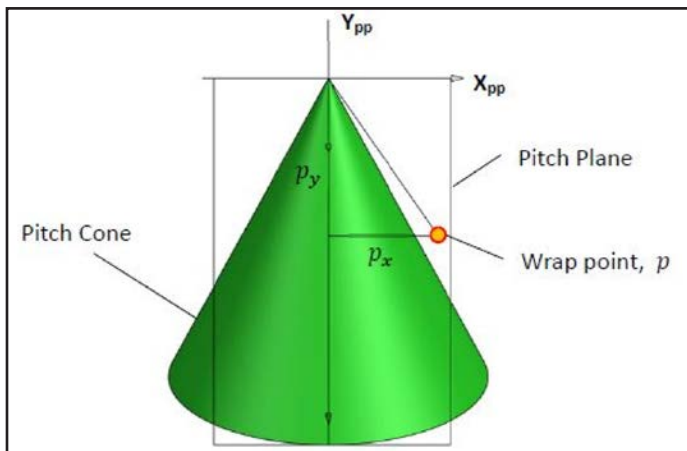


Figure 5 Normal view to pitch plane displaying wrap point.

Calculate the rotation angle that the point will wrap around the cone, (28)

$$\theta_p = \frac{1}{\sin \Gamma} \tan^{-1} \frac{p_x}{p_y}$$

Calculate the radius of the cone at location, z_p , (29)

$$R_p = z_p \tan \Gamma$$

Convert the cylindrical coordinates for the wrap point into global Cartesian coordinates. (30)

$$x_p = R_p \cos \theta_p \quad (31)$$

$$y_p = R_p \sin \theta_p$$

Therefore, all the local cutter positions can be wrapped and transformed into the global Cartesian coordinate system.

Calculating Local Cutter Coordinate System

Since AGMA 929 effectively calculates the normal circular tooth thicknesses at a specific spot along the cutter path, the next step is to determine the correct orientation of the normal plane. A complete coordinate system will be oriented to have the $x_n y_n$ plane normal to the cutter path, with the origin at each global coordinate of the cutter path calculated previously; this coordinate system will be called C_n .

Tangent axis, z_n . The tangent axis is defined by a vector that is tangent to the cutter sweep path at the location of the wrapped point. There are a couple of options for calculating this tangent vector. One could calculate the first derivative of the cutter sweep path formulas for both face milling and face hobbing so that the slope anywhere along that path can be predicted. Once that is accomplished a vector can be constructed in three dimensions to describe this tangent axis.

Since many assumptions are made throughout this method, the simplest method for calculating an approximate tangent vector is using finite difference; the finite difference method is described in the following equation: (32)

$$f'(x) = \lim_{\Delta x \rightarrow 0} \left(\frac{f(x + \Delta x) - f(x)}{\Delta x} \right)$$

It is difficult to determine the correct size of Δx that will approximate the tangent close enough for this method. Since the cutter sweep path is smooth and continuous for all locations

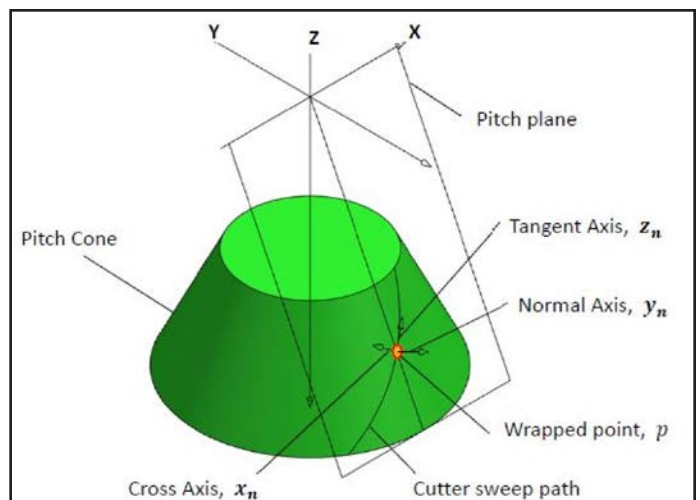


Figure 6 Definition of a wrapped point's local coordinate system.

along the arc, it is possible to quantify the error of our approximation using a Taylor expansion. This is beyond the scope of this document, but is mentioned here for further exploration.

The practical approach to applying the finite difference method is to calculate a neighboring wrapped point along the cutter sweep path for each wrapped calculation point. A vector can then be defined by passing through both sweep path points. As the points become closer and closer the vector connecting the two points approaches a tangent line.

Normal axis— y_n . The normal vector is defined as a vector radiating perpendicularly from the surface of the right cone at the wrapped point location (Fig. 6). The normal vector at wrap point $p = (p_x, p_y, p_z)$ can be calculated by the following equation:

$$y_n = (2p_x \cos^2 \Gamma, 2p_y \cos^2 \Gamma, -2p_z \sin^2 \Gamma) \tag{33}$$

A brief derivation will follow to explain the calculation of the normal axis. The general function of a right cone,

$$C(x, y, z) = (x^2 + y^2) \cos^2 \Gamma - z^2 \sin^2 \Gamma \tag{34}$$

A gradient, ∇u , is always normal to a function when,

$$\nabla_u = u_x e_x + u_y e_y + u_z e_z \tag{35}$$

Where,

$$e_x = \langle 1, 0, 0 \rangle \tag{36}$$

$$e_y = \langle 0, 1, 0 \rangle \tag{37}$$

$$e_z = \langle 0, 0, 1 \rangle \tag{38}$$

Let,

$$u(x, y, z) = x^2 \cos^2 \Gamma + y^2 \cos^2 \Gamma - z^2 \sin^2 \Gamma \tag{39}$$

Therefore,

$$\nabla_u = \langle 2x \cos^2 \Gamma, 2y \cos^2 \Gamma - 2z \sin^2 \Gamma \rangle \tag{40}$$

The cross vector will complete the definition of the local Cartesian coordinate system. This vector is calculated by taking the cross product of the tangent vector and the normal vector.

$$x_n = z_n y_n \tag{41}$$

After calculating all the vector directions for the local coordinate system, all three of the vectors should be normalized.

Normal Circular Tooth Thickness Calculations

Generalizing AGMA 929-A06. As previously discussed AGMA 929-A06 utilizes the technique of converting the spiral bevel gear tooth to a virtual spur gear tooth to calculate the top lands at the toe, mean, and heel; the equations presented in AGMA 929-A06 are unique for each of these points of interest. General equations can be derived from AGMA 929-A06 so that the tooth thickness can be calculated anywhere along the profile and lengthwise direction. The generalized formulas for the conversion to a virtual spur gear are presented here (Fig. 7). Also, a handful of helpful formulas for calculating some spiral gear tooth geometry with respect to cone distance, A_μ , are developed. The cone distance range variable must correlate to the cone distances first chosen in the cutter path sections.

The notation in this section utilizes the terminology as if the member being modeled is the gear. Unless specifically specified

the gear terminology should be replaced with pinion terminology in the formulas if the pinion is the part being modeled.

Spiral angle for face milling with respect to cone distance,

$$\psi(A_\mu) = \sin^{-1} \frac{2A_m R_c \sin \psi_m - A_m^2 + A_\mu^2}{2A_\mu R_c} \tag{42}$$

Generating angle for face hobbing with respect to cone distance,

$$q(A_\mu) = \cos^{-1} \frac{A_\mu^2 + S_1^2 - R_c^2}{2A_\mu S_1} \tag{43}$$

Spiral angle for face hobbing with respect to cone distance,

$$\Psi(A_\mu) = \tan^{-1} \frac{A_\mu - Q \cos q(A_\mu)}{Q \sin q(A_\mu)} \tag{44}$$

Slot width with respect to cone distance for the gear member,

$$W_G(A_\mu) = W_c \left[1 - \frac{A_\mu \cos \psi(A_\mu)}{A_m \cos \psi_m} \right] + \frac{A_\mu}{A_m} [t_{mp} \cos \psi(A_\mu)] - \left[\frac{A_\mu \cos \psi(A_\mu)}{A_m \cos \psi_m} b_G (\tan \Phi_1 - \tan \Phi_2) \right] + \frac{A_\mu \cos \psi(A_\mu)}{A_o \cos \psi(A_o)} \frac{B}{\cos \frac{\Sigma \Phi}{2}} + (A_m - A_\mu) (\tan \Phi_1 - \tan \Phi_2) \tan \xi \tag{45}$$

Slot width with respect to cone distance for the pinion member,

$$W_P(A_\mu) = \frac{A_\mu \cos \psi(A_\mu)}{A_m \cos \psi_m} p_n - \Sigma b_\mu (\tan \Phi_1 - \tan \Phi_2) - W_G(A_\mu) + \frac{A_\mu \cos \psi(A_\mu)}{A_o \cos \psi(A_o)} \frac{B}{\cos \frac{\Sigma \Phi}{2}} \tag{46}$$

Normal pitch radius with respect to cone distance (substitute proper pitch diameter and pitch angle for member to model),

$$r_N(A_\mu) = \frac{D A_\mu}{2 \cos \Gamma \cos^2 \psi_m A_o} \tag{47}$$

Normal base radius with respect to cone distance, concave,

$$r_{bN1}(A_\mu) = r_N(A_\mu) \cos \Phi_1 \tag{48}$$

Normal base radius with respect to cone distance, convex,

$$r_{bN2}(A_\mu) = r_N(A_\mu) \cos \Phi_2 \tag{49}$$

Figure 7 displays the base radii graphically. The value of r_{bN1} and r_{bN2} are shown as the same value because the pressure angle of the concave and convex flanks are the same. This is typical but not mandatory for bevel gears without a hypoid offset.

Normal pinion circular tooth thickness at pitch line with respect to cone distance,

$$t_{NP}(A_\mu) = b_G(A_\mu) (\tan \Phi_1 - \tan \Phi_2) - W_G(A_\mu) - \frac{A_\mu \cos \psi(A_\mu)}{A_o \cos \psi(A_o)} \frac{B}{\cos \frac{\Sigma \Phi}{2}} \tag{50}$$

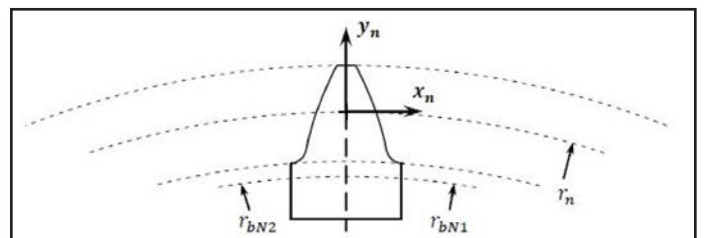


Figure 7 Definition of the geometry of the virtual spur gear in the normal plane.

Normal gear circular tooth thickness at pitch line with respect to cone distance,

$$t_{NG}(A_\mu) = b_p(A_\mu)(\tan \Phi_1 - \tan \Phi_2) + W_G(A_\mu) - \frac{A_\mu \cos \Psi(A_\mu)}{A_o \cos \Psi(A_o)} \frac{B}{\cos \frac{\Sigma \Phi}{2}} \quad (51)$$

Normal working radius with respect to cone distance,

$$r_{wN}(A_\mu) = r_N(A_\mu) + w \quad (52)$$

Where

w is a range variable for calculating the working radius. The valid range for w is,

$$-b(A_\mu) \leq w \leq a(A_\mu) \quad (53)$$

Pressure angle at working radius with respect to cone distance, concave,

$$\Phi_{1w}(A_\mu) = \cos^{-1} \frac{r_{bN1}(A_\mu)}{r_{wN}(A_\mu)} \quad (54)$$

Pressure angle at working radius with respect to cone distance, convex,

$$\Phi_{2w}(A_\mu) = \cos^{-1} \frac{r_{bN2}(A_\mu)}{r_{wN}(A_\mu)} \quad (55)$$

Normal circular tooth thickness for pinion at working radius with respect to cone distance,

$$t_{wNP}(A_\mu) = \left[\frac{t_{NP}(A_\mu)}{r_N(A_\mu)} + \text{inv} \Phi_1 - \text{inv} \Phi_{1w} + \text{inv}(-\Phi_2) - \text{inv} \Phi_{2w} \right] r_{wN}(A_\mu) \quad (56)$$

Normal circular tooth thickness for gear at working radius with respect to cone distance,

$$t_{wNG}(A_\mu) = \left[\frac{t_{NG}(A_\mu)}{r_N(A_\mu)} + \text{inv} \Phi_1 - \text{inv} \Phi_{1w} + \text{inv}(-\Phi_2) - \text{inv} \Phi_{2w} \right] r_{wN}(A_\mu) \quad (57)$$

Certain designs have the dedendum plunge below the virtual gear's base radius; when this occurs, the normal circular tooth thickness will become a complex number. Only the real portion of this value should be used when recording the answers.

Converting thicknesses to coordinates. The tooth thickness calculations shown earlier in *Generalizing AGMA 929-A06* is a circular tooth thickness positioned at a specified working radius. The local coordinate system has the origin located where the pitch radius crosses the center of the tooth thickness (Fig. 7). For each working radius used the calculated circular tooth thicknesses need to be converted to chordal thicknesses before they can be recorded as Cartesian coordinates.

Normal chordal tooth thickness for pinion at working radius with respect to cone distance,

$$t_{wcNP}(A_\mu) = 2r_{wN}(A_\mu) \sin \frac{t_{wNP}(A_\mu)}{2r_{wN}(A_\mu)} \quad (58)$$

Normal chordal tooth thickness for gear at working radius with respect to cone distance,

$$t_{wcNG}(A_\mu) = 2r_{wN}(A_\mu) \sin \frac{t_{wNG}(A_\mu)}{2r_{wN}(A_\mu)} \quad (59)$$

Now that the circular thickness has been converted to a chordal thickness, a small correction is needed to the location of the thickness in the profile direction (along y_n). Figure 8 depicts

this correction and provides a visual explanation why this correction is required. The working radius is equal to the pitch radius in the figure, and its relative radius has been decreased to exaggerate the size of the correction in the figure.

Pinion shift factor at working distance with respect to cone distance,

$$y_{wsP}(A_\mu) = r_{wN}(A_\mu) \left[1 - \cos \frac{t_{wNP}(A_\mu)}{2r_{wN}(A_\mu)} \right] \quad (60)$$

Gear shift factor at working distance with respect to cone distance,

$$y_{wsG}(A_\mu) = r_{wN}(A_\mu) \left[1 - \cos \frac{t_{wNG}(A_\mu)}{2r_{wN}(A_\mu)} \right] \quad (61)$$

Local Cartesian coordinates for the pinion with respect to cone distance,

$$pt_{1P} = \left(\frac{t_{wcNP}(A_\mu)}{2}, w - y_{wsP}(A_\mu) \right) \quad (62)$$

$$pt_{2P} = \left(\frac{t_{wcNP}(A_\mu)}{2}, w - y_{wsP}(A_\mu) \right) \quad (63)$$

Local Cartesian coordinates for the gear with respect to cone distance,

$$pt_{1G} = \left(\frac{t_{wcNG}(A_\mu)}{2}, w - y_{wsG}(A_\mu) \right) \quad (64)$$

$$pt_{2G} = \left(-\frac{t_{wcNG}(A_\mu)}{2}, w - y_{wsG}(A_\mu) \right) \quad (65)$$

Transform the Local Normal Tooth Thicknesses to Global

To this point all the tooth thickness points are defined relative to a local coordinate system. The global location for each one of these local coordinate systems are known, but to complete the model, all points describing the tooth flanks must be known

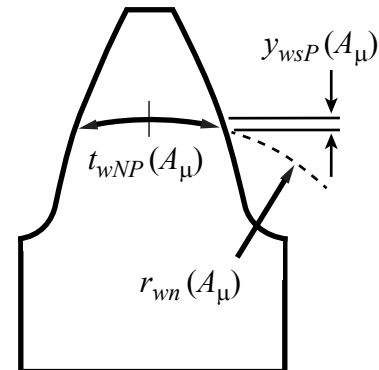


Figure 8 Shift factor when converting circular to chordal thicknesses (pinion shown).

relative to the global coordinate system. This is accomplished using a coordinate transformation matrix, C_T :

$$C_T = C_n C_G \quad (66)$$

Where,

C_G is a 3x3 identity matrix that describes the global coordinate system. See Coordinate System Definition for a more detailed explanation. Once a vector, V_p , relative to the local

coordinate system, C_n , is constructed that passes through a calculated tooth flank point, the transformation can be calculated:

$$V_G = C_T V_P \tag{67}$$

Where,

V_G is a vector that passes through the exact same flank point, but is described relative to the global coordinate system.

Results

Now that the method is complete, the next logical step is to determine just how accurate this model is when compared to the theoretical geometry of a spiral bevel gear. This method is strictly approximate; many caveats have been discussed in the previous sections. To accomplish a comparison between this method and a theoretical part there must be a reliable standard by which to compare it. Comparing the calculated points from this method with a physical, cut part would introduce potential variations from the manufacturing process. For this reason alone it was decided to compare the calculated points to a different, yet trusted, mathematical model. Gleason Works has developed a commercial software package — *T900* — that generates an accurate point cloud describing the geometry of the tooth flank and fillet condition of bevel gears and pinions. While the purpose of this software is far greater than just the generation of a point cloud, the other functionality is beyond the scope of this document. The point cloud produced from *T900* can be imported into a CAD package to assist in the generation of the

Table 1 Basic spiral geometry of model		
	Pinion	Gear
Number of teeth	11	57
Face width	2.0	2.0
Diametral pitch	4.0	
Shaft angle	Non 90°	

exact geometry produced by the machine settings for a particular design. The point cloud represents the standard as to which this method is compared.

The member chosen for this analysis is a left-hand spiral bevel gear generated by face mill completing.

Some of the basic geometry has been provided in Table 1, but the exact details of the geometry are relatively unimportant. An angular set was chosen as this method has no shaft angle restrictions.

The output from *T900* is a point cloud that describes the flanks of a spiral bevel or hypoid gear set. A gear tooth is divided into a 13- (profile) by-10 (length) grid for each flank; therefore 260 unique points describe each tooth. For this analysis these discrete points were bridged together using Siemens *NX 8.5* CAD software. The point cloud was connected in the profile and lengthwise direction with curves generated by a cubic, polynomial regression. Once the lattice of curves is generated the curves are used as ribs to create a bi-cubic surface. Figure 9 shows the tooth surface generated from the *T900* point cloud in gray.

The face width of the part is broken into 10 segments for the calculation; addendum and dedendum

are also broken into 10 segments. The part being modeled has a short addendum and long dedendum. Figure 10 shows the calculated points and solid model sectioned through the normal plane (Fig. 9) of a tooth. The calculated points go beyond the root line of the model because the calculated points were generated to the base circle radius of the virtual spur gear. When doing the comparison the last four points of each profile will be omitted, as they fall below the root fillet tangency point.

A linear measurement normal to the *T900* surface to each calculated point is used to measure the deviation between the calculated points and the surface. The normal tooth thicknesses at the toe and heel will be omitted in the comparison, as these points are beyond the bounds of the *T900* surface. The absolute values of the measured deviations for each flank are given (Tables 2 and 3).

The red values are measured deviations that exceed one one-thousandth of an inch. Overall, the results depict a model that very closely approximates the flanks predicted by the Gleason Works *T900* software. The average deviation for each normal cross-section in the lengthwise direction is displayed in Table 4.

Conclusion

The purpose of this presentation is to describe a procedure for calculating a very close approximation of the geometry of a spiral bevel gear tooth.

This method is built upon the techniques and formulas described in AGMA 929-A06.

The second portion of the document compared the results of this method with the results from a proven Gleason software package.

The results are extremely close.

Many models have been generated since this original case study, and the subsequent models correlate well with the geometry predicted by Gleason software.

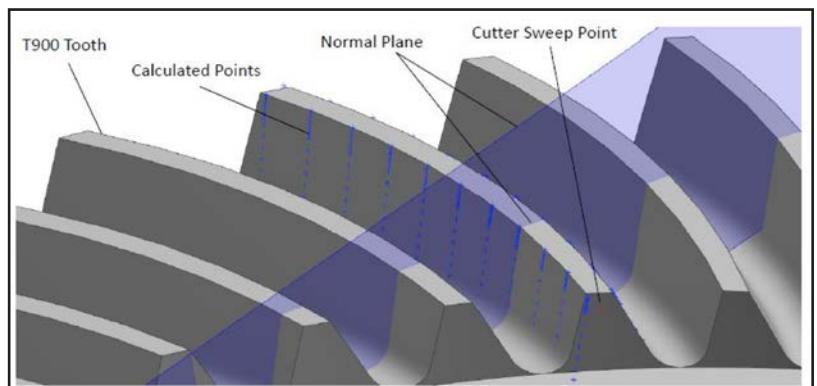


Figure 9 Calculated points overlaid on a tooth modeled using Gleason T900.

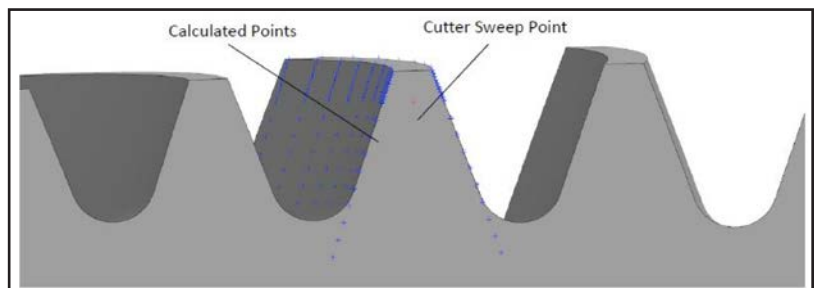



Figure 10 Calculated points in the normal plane.

The model described throughout this document should not be used for advanced analysis (i.e., finite element or the like), as the models created from this method do not have any modifications to the tooth flanks to adjust or optimize the tooth contact pattern.

At present AGMA's Bevel Gear Committee is working on revising the formulas in AGMA 929-A06 to adopt the generalized formulas described here. The technique of utilizing generalized formulas will expand the capabilities of AGMA 929. 

References

1. Baxter, Jr., M.L. *Spiral Bevel Gear Theory*, Unpublished. 1963.
2. AGMA 929-A06. *Calculation of Bevel Gear Top Land and Guidance on Cutter Edge Radius*.
3. Colbourne, J.R. *The Geometry of Involute Gears*, Springer-Verlag, New York, 1987.
4. ANSI/AGMA 2005-D03. *Design Manual for Bevel Gears*.
5. Grant, G.B. *A Treatise on Gear Wheels*, 21st Edition. Philadelphia Gear Works Inc., Philadelphia, 1980.
6. Khiralla, T.W. *On the Geometry of External Involute Spur Gears*, C/I Leaming, North Hollywood, California, 1976.
7. Krenzer, T. *The Bevel Gear*, 2007.
8. Litvin, F.L. *Theory of Gearing*, NASA Reference Publication; 1212 (AVSCOM Technical Report; 88-C-035), 1989.
9. *NX 8.5 Help Documentation*. Siemens Product Lifecycle Management Software Inc., 2012.
10. Shtipelman, B.A. *Design and Manufacture of Hypoid Gears*, John Wiley and Sons, Inc. 1978.
11. *T900 User's Manual*. Gleason Works.

For Related Articles Search

bevel gear geometry 
at www.geartechnology.com

After graduating from Northern Illinois University in 2010 with a bachelors' in mechanical engineering, **Brendan Bijonowski** has pursued a career in design. In 2011 he joined the engineering ranks of Arrow Gear Company, located in Downers Grove, IL as a design engineer. His passion for the geometry of gearing and attention to detail can clearly be seen in all of his work. Bijonowski is a member of the AGMA Bevel Gear Committee, where he works on defining geometry and improving rating methods. He is also a member of the AGMA Computer Programming Committee, where he applies his experience and knowledge as a gear engineer to an ever-growing collection of technical software.



		Heel										Toe
		0	1	2	3	4	5	6	7	8	9	10
Topland	0		0.927	0.938	0.949	0.963	0.969	0.956	0.927	0.899		
	1		0.249	0.214	0.188	0.174	0.154	0.109	0.035	0.046		
	2		0.305	0.258	0.223	0.201	0.173	0.121	0.042	0.047		
	3		0.358	0.302	0.257	0.226	0.189	0.130	0.045	0.049		
	4		0.411	0.343	0.289	0.249	0.205	0.138	0.045	0.054		
	5		0.461	0.384	0.319	0.270	0.218	0.143	0.043	0.061	0.158	
	6		0.051	0.422	0.348	0.289	0.230	0.146	0.038	0.070	0.171	
	7		0.558	0.459	0.375	0.307	0.241	0.148	0.032	0.080	0.186	
	8		0.603	0.494	0.401	0.323	0.249	0.148	0.025	0.092	0.201	
	9		0.647	0.528	0.425	0.337	0.257	0.147	0.018	0.104	0.218	
Pitch	10		0.689	0.559	0.447	0.350	0.262	0.146	0.010	0.116	0.235	
	11		0.839	0.671	0.522	0.396	0.268	0.125	0.039	0.205	0.360	
	12		0.952	0.744	0.555	0.381	0.215	0.024	0.186	0.387	0.575	
	13		1.023	0.077	0.526	0.299	0.113	0.098	0.324	0.546	0.765	
	14		1.049	0.759	0.523	0.350	0.015	0.291	0.644	1.046	1.345	
	15		1.024	0.423	0.298	0.190	0.418	0.754	0.950	0.467	1.259	
Root	16		0.913	0.000	0.052	0.103	0.539					
	17											
	18											
	19											
	20											

		Heel										Toe
		0	1	2	3	4	5	6	7	8	9	10
Topland	0			0.342	0.344	0.326	0.307	0.313	0.373	0.377		
	1		0.296	0.327	0.340	0.332	0.320	0.334	0.371	0.405		
	2		0.268	0.311	0.334	0.335	0.331	0.353	0.397	0.436		
	3		0.238	0.292	0.325	0.336	0.341	0.370	0.421	0.465		
	4		0.206	0.271	0.315	0.335	0.348	0.385	0.442	0.493	0.538	
	5		0.171	0.248	0.302	0.332	0.354	0.398	0.462	0.518	0.566	
	6		0.135	0.222	0.288	0.328	0.358	0.409	0.479	0.542	0.593	
	7		0.096	0.195	0.271	0.321	0.360	0.419	0.495	0.565	0.619	
	8		0.056	0.166	0.252	0.312	0.360	0.427	0.510	0.586	0.643	
	9		0.013	0.135	0.232	0.302	0.359	0.433	0.523	0.605	0.667	
Pitch	10		0.031	0.102	0.210	0.289	0.356	0.438	0.534	0.623	0.690	
	11		0.231	0.055	0.094	0.212	0.318	0.442	0.581	0.702	0.817	
	12		0.460	0.243	0.054	0.102	0.246	0.402	0.562	0.729	0.864	
	13		0.710	0.467	0.254	0.042	0.140	0.328	0.542	0.746	0.938	
	14		0.983	0.690	0.416	0.186	0.230	0.281	0.566	0.705	0.840	
	15		1.285	0.911	0.615	0.389	0.158	0.008	0.101	0.526	1.220	
	16		1.559	1.321	1.114	0.765	0.403					
	17											
	18											
	19											
Root	20											

Flank	Heel	0	1	2	3	4	5	6	7	8	9	10
Concave		0.695	0.486	0.394	0.318	0.277	0.277	0.213	0.267	0.498		
Convex		0.510	0.370	0.339	0.308	0.299	0.359	0.458	0.564	0.750		